Available online at www.sciencedirect.com
SCIENCE DIRECT®
ELSEVIER
International Journal of Solids and Structures 43 (2006) 551–568
INTERNATIONAL JOURNAL OF SOLIDS and STRUCTURES
www.elsevier.com/locate/ijsolstr

Postbuckling analysis of elastic shells of revolution considering mode switching and interaction

J.G. Teng *, T. Hong

Department of Civil and Structural Engineering, The Hong Kong Polytechnic University, Kowloon, Hong Kong, China

Received 23 September 2004; received in revised form 18 June 2005
Available online 19 August 2005

Abstract

The postbuckling response of shells is known to exhibit complex phenomena including mode switching and interaction, particularly in the advanced postbuckling range. The existing literature contains many initial postbuckling analyses as well as advanced postbuckling analyses for a single buckling mode, but little work is available on the advanced postbuckling analysis of shells of revolution considering mode switching and interaction. In this paper, a numerical method for the advanced postbuckling analysis of thin shells of revolution subject to torsionless axisymmetric loads is presented, in which such mode switching and interaction are properly captured. Numerical results obtained using the present method for several typical problems not only demonstrate the capability of the method, but also lead to significant observations concerning the postbuckling behavior of thin shells of revolution. In particular, the results show that strong interaction between different harmonic modes may exist and the transition of deformation mode from one to another is gradual. Consequently, the conventional approach of finding the postbuckling path of a shell as the lower festoon curve of postbuckling paths of individual harmonic modes is not valid and is at best a convenient approximation.

Keywords: Shells; Shells of revolution; Postbuckling; Mode switching; Mode interaction

1. Introduction

Axisymmetric shells are widely used in many engineering fields. Examples include aircraft, spacecraft, submarines, nuclear reactors, cooling towers, storage silos and tanks, roof domes, offshore platforms,

* Corresponding author. Tel.: +852 2766 6012; fax: +852 2334 6389.
E-mail address: cejgteng@polyu.edu.hk (J.G. Teng).

0020-7683/$ - see front matter © 2005 Elsevier Ltd. All rights reserved.
doi:10.1016/j.ijsolstr.2005.06.060

tubular towers, chimneys, pressure vessels and pipelines. A perfect shell of revolution under axisymmetric loads may bifurcate into a non-symmetric mode at a suitable level of loading. The load carrying capacity of a corresponding real shell depends not only on the bifurcation load, but also on the nature of the post-bifurcation path, which determines the sensitivity of the shell to initial geometric imperfections. As a result, the postbuckling behavior of perfect shells has been of enormous interest to shell stability researchers and designers. Nevertheless, postbuckling analysis of perfect shells has been and still remains a challenge to numerical analysts, because the postbuckling behavior of perfect shells may be highly unstable and very complicated, and may involve complex mode switching and interaction. It should be noted that some of the difficulties encountered in the postbuckling analysis of perfect shells abate or disappear when significant geometric imperfections of a suitable form are included in the analysis. In this sense, an analysis of the post-buckling behavior of perfect shells is more challenging than a nonlinear analysis of imperfect shells for which the phenomena of bifurcation and mode switching are likely to be eroded by the presence of significant geometric imperfections. This paper is concerned only with perfect shells, whose postbuckling behavior is important in its own right and for a proper understanding of the sensitivity of the shell to geometric imperfections.

The existing literature on postbuckling behavior contains many initial postbuckling analyses (e.g. Budiansky and Hutchinson, 1966; Koiter, 1945). A number of researchers have also implemented the general theory of initial postbuckling in finite element analyses of axisymmetric shells (e.g. Azrar et al., 1993; Endou et al., 1976; Flores and Godoy, 1992, 1993). However, these studies were able to predict only the initial part of the postbuckling path. Rigorous analytical studies (e.g. Esslinger and Geier, 1975; Shen, 1996; Shen and Chen, 1991; Yamaki, 1984) have also examined advanced postbuckling responses, but these analyses were concerned with postbuckling deformations in a single buckling mode, so mode switching and interaction were not considered. More recently, Bulenda (1993) presented a harmonic-by-harmonic finite element method to compute the postbuckling path of a cylindrical shell under uniform external pressure, but mode switching was again not considered. Similarly, Combescure's (1999) results for the postbuckling of an elastic–plastic shell with significant imperfections under external pressure were not concerned with mode switching. He did not observe any mode change in his static results, but noticed such a change in his dynamic results and attributed this to inertial effects. The best investigation so far appears to be that by Kato et al. (1997) who studied the secondary postbuckling behavior and mode interaction in spherical caps under uniform external pressure. Although secondary bifurcation was considered in their study by monitoring the eigenvalue of a chosen secondary bifurcation mode, the choice of this mode appears to be arbitrary apart from the exclusion of those describing the primary post-bifurcation path. As a result, mode switching was not properly captured. Only spherical caps with the first and second bifurcation points being almost coincidental were studied, so the capability of the method for other situations is not clear.

The modelling of mode switching is very challenging, and there have been a number of recent attempts using general shell elements either employing a static approach or a dynamic approach (Choong and Ramm, 1998; Guggenberger, 1996; Kusher, 1997; Riks et al., 1996). These studies are still exploratory, with only limited successes. There appears to have been no previous study using axisymmetric shell elements which properly modelled the advanced postbuckling deformation process of perfect elastic shells of revolution involving continuous mode switching and interaction.

In this paper, a numerical method for the advanced postbuckling analysis of elastic shells of revolution subject to torsionless axisymmetric loads is presented, based on the general formulation for nonlinear non-symmetric deformations of shells of revolution presented in Hong and Teng (2002). The method is based on the use of small load-disturbances in a nonlinear analysis of shells of revolution under general non-symmetric loads, and is referred to as the load-disturbance method. By specifying small load-disturbances in appropriate harmonic modes, complex postbuckling paths with mode switching and interaction can be predicted. Numerical results of a number of typical problems solved using this method are presented to demonstrate its accuracy and capability.

2. Nonlinear equations of postbuckled shells

2.1. Displacements of postbuckled shells

The isoparametric doubly curved thin shell element used in the present finite element formulation is shown in Fig. 1. The accuracy of the element has been demonstrated in many successful applications (Hong and Teng, 2002; Teng and Rotter, 1989a,b). The element geometry is described in cylindrical coordinates and is uniquely defined by the radius R, the axial coordinate z and the element meridional curvature $\mathrm{d}\varphi/\mathrm{d}s$ at the nodal points. The intermediate values of coordinates R, z, and $\mathrm{d}\varphi/\mathrm{d}s$ of the shell element are interpolated in terms of the nodal coordinates using cubic Hermitian functions. The nodal displacements in global coordinates are taken as u_i, $(\mathrm{d}u/\mathrm{d}s)_i$, v_i, $(\mathrm{d}v/\mathrm{d}s)_i$, w_i and $(\mathrm{d}w/\mathrm{d}s)_i$ at the two nodes of the element

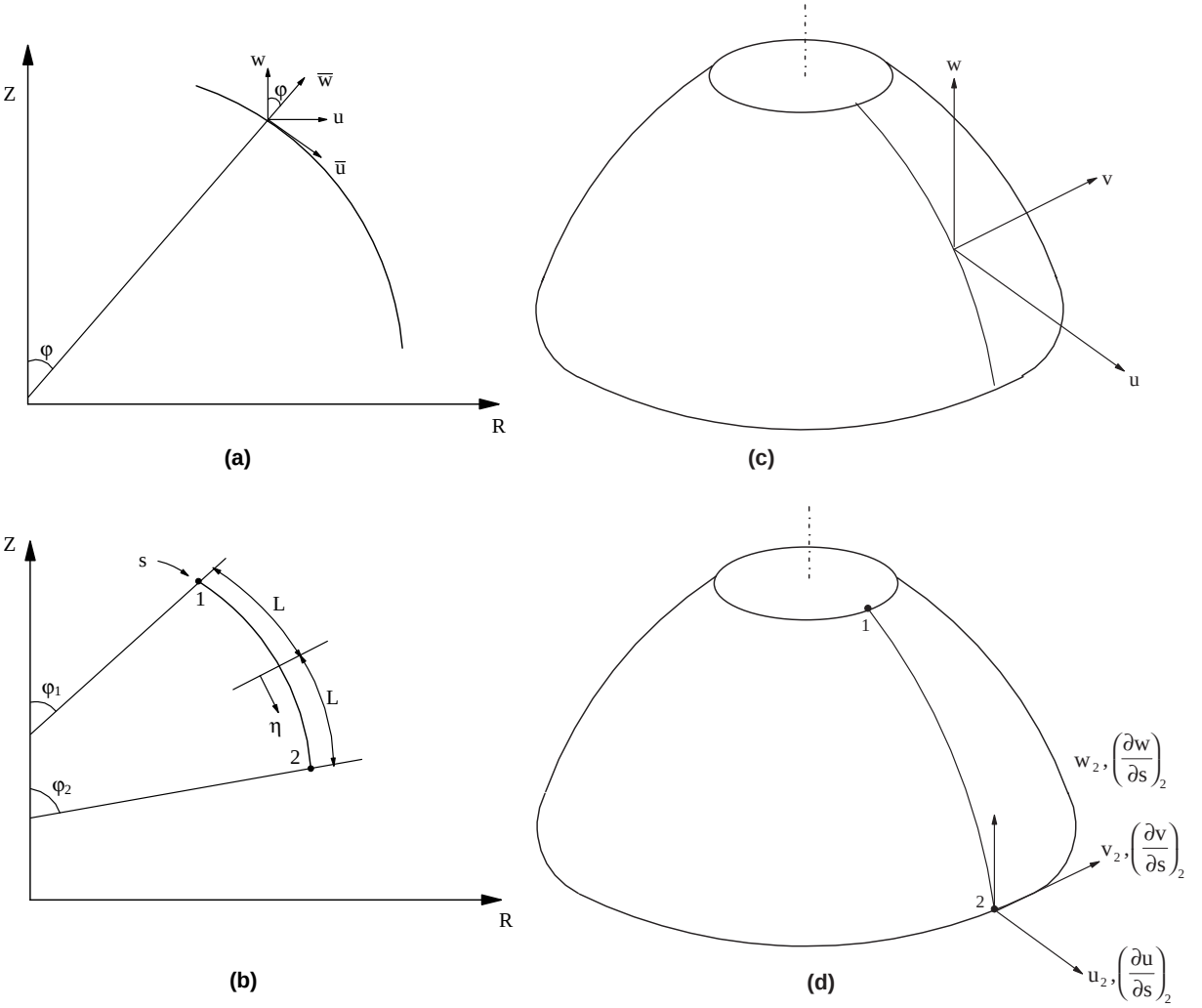

Fig. 1. The doubly curved axisymmetric shell element. (a) Local and global displacements. (b) Geometry of an element. (c) Displacements within the element. (d) Nodal displacements.

(Fig. 1d). The displacements at any point, defined in the global coordinate system, u, v and w (Fig. 1c) are interpolated between the nodal points in terms of the nodal values also using cubic Hermitian functions. The set of global displacements u, v and w at any point is related by a transformation matrix $[T]$ to the local displacements $\bar{u}$, $\bar{v}$ and $\bar{w}$ (in curvilinear coordinates) (Teng and Rotter, 1989a).

For a shell of revolution subject to torsionless axisymmetric loads, pre-buckling displacements are axisymmetric. The postbuckling displacements differ from the pre-buckling displacements in that they include both axisymmetric components u_0, v_0 and w_0 and non-axisymmetric components $u_i \cos n_i\theta$, $v_i \sin n_i\theta$ and $w_i \cos n_i\theta$. If several buckling modes correspond to similar buckling loads such that all these non-symmetric modes are involved in postbuckling deformations, these modes are said to interact in the postbuckling process and should be included in an accurate postbuckling analysis. In addition, due to the nonlinear coupling effects between these buckling modes, deformations in additional harmonic modes arise during the postbuckling process. For a detailed treatment of the nonlinear coupling effects and particularly the determination of harmonic modes from nonlinear coupling, readers are referred to Hong and Teng (2002). The postbuckling displacements including interacting buckling modes as well as additional deformation modes due to nonlinear coupling are described by

$$\begin{aligned} u &= u_0 + \sum_{i=1}^{N} u_i \cos n_i\theta \\ v &= v_0 + \sum_{i=1}^{N} v_i \sin n_i\theta \\ w &= w_0 + \sum_{i=1}^{N} w_i \cos n_i\theta \end{aligned} \tag{1}$$

in which θ is the circumferential angular coordinate, N is the number of the involved buckling modes and n_i is the harmonic number or wave number of the ith harmonic mode which is referred to as harmonic mode n_i.

2.2. Nodal variables

For postbuckling displacements defined by Eq. (1), the vector of nodal variables for each element is

$$\{\delta\}_e = \{\delta_0, \cdots, \delta_i, \ldots, \delta_N\}^T \tag{2a}$$

in which

$$\delta_i = \left\{ u_1^i, \left(\frac{\partial u}{\partial s}\right)_1^i, v_1^i, \left(\frac{\partial v}{\partial s}\right)_1^i, w_1^i, \left(\frac{\partial w}{\partial s}\right)_1^i, u_2^i, \left(\frac{\partial u}{\partial s}\right)_2^i, v_2^i, \left(\frac{\partial v}{\partial s}\right)_2^i, w_2^i, \left(\frac{\partial w}{\partial s}\right)_2^i \right\}^T \tag{2b}$$

where δ_0 denotes the axisymmetric terms and δ_i ($i = 1, \ldots, N$) denotes the non-axisymmetric terms of the ith harmonic, and the subscripts 1 and 2 are the nodal point numbers of the element.

If the postbuckling analysis is carried out assuming that only one non-symmetric mode is involved, the postbuckling displacements (Eq. (1)) reduce to

$$\begin{aligned} u &= u_0 + u_n \cos n\theta \\ v &= v_0 + v_n \sin n\theta \\ w &= w_0 + w_n \cos n\theta \end{aligned} \tag{3}$$

in which n is the wave number of the bifurcation buckling mode or any other chosen mode. Therefore, the vector of nodal variables for each element is

$$\{\delta\}_e = \left\{ u_{01}, \left(\frac{\partial u_0}{\partial s}\right)_1, v_{01}, \left(\frac{\partial v_0}{\partial s}\right)_1, w_{01}, \left(\frac{\partial w_0}{\partial s}\right)_1, u_{02}, \left(\frac{\partial u_0}{\partial s}\right)_2, v_{02}, \left(\frac{\partial v_0}{\partial s}\right)_2, w_{02}, \left(\frac{\partial w_0}{\partial s}\right)_2, \right.$$
$$\left. u_{n1}, \left(\frac{\partial u_n}{\partial s}\right)_1, v_{n1}, \left(\frac{\partial v_n}{\partial s}\right)_1, w_{n1}, \left(\frac{\partial w_n}{\partial s}\right)_1, u_{n2}, \left(\frac{\partial u_n}{\partial s}\right)_2, v_{n2}, \left(\frac{\partial v_n}{\partial s}\right)_2, w_{n2}, \left(\frac{\partial w_n}{\partial s}\right)_2 \right\}^T \quad (4)$$

in which the subscript 0 denotes axisymmetric deformations and the subscript n denotes non-symmetric deformations in harmonic mode n.

The postbuckling path determined considering the coupling and/or interaction of a number of harmonic modes is referred to as the postbuckling path for harmonic modes $n_1 + n_2 + \cdots + n_i + \cdots + n_N$ or simply for $n = n_1 + n_2 + \cdots + n_i + \cdots + n_N$. The plus sign is thus used to mean that these modes are coupled or interact in the analysis. When only a single harmonic mode n_i is considered, the predicted postbuckling path is referred to as the postbuckling path for harmonic mode n_i or simply for $n = n_i$. It should be noted that axisymmetric displacements are generally present during postbuckling deformations, although this is not explicitly stated in the terminology suggested above.

2.3. Governing nonlinear equations

The equations governing the nonlinear deformations of shells of revolution under non-symmetric loads (Hong and Teng, 2002) can be specialized for the non-symmetric deformations of postbuckled shells with the nodal variables defined by Eq. (2). The total Lagrangian approach is adopted here in which all the quantities are referred to the undeformed configuration. The application of the principle of virtual displacements leads to a set of nonlinear equations for the finite element model of a given structure which may be represented by

$$\{\Phi(\delta)\} = \{F\} - \sum_{\text{element}} \int [B]^T \{\Sigma\} \, dV = 0 \quad (5)$$

in which $\{\delta\}$ is the vector of nodal displacement variables, {F} is the vector of equivalent nodal forces due to body forces and surface tractions, $[B]$ is the incremental strain–displacement matrix based on the nonlinear shell theory of Rotter and Jumikis (1988) for thin shells of revolution which is a special case of the general nonlinear thin shell theory of Teng and Hong (1998), $\{\Sigma\}$ is the vector of generalized stress resultants and $\{\Phi(\delta)\}$ is a vector of nodal residual forces. For each iteration, the nodal displacement increments for the structure $\{\Delta\delta\}$ are obtained by solving the following linearised system of equations

$$\{\Phi(\delta)\} = [K_T]\{\Delta\delta\} \quad (6)$$

where $[K_T]$ is termed the global tangent stiffness matrix. The tangent stiffness matrix for each element is given by

$$[K_T]_e = [K]_e + [K_\sigma]_e \quad (7)$$

where $[K]_e$ is the stiffness matrix including the effect of changes in geometry, and $[K_\sigma]_e$ accounts for the effect of internal stresses. These two matrices $[K]_e$ and $[K_\sigma]_e$ are given in Hong and Teng (2002).

The element tangent stiffness matrices $[K_T]_e$ (Eq. (7)) are condensed to reduce the inter-element discontinuity in a way similar to that described in Teng and Rotter (1989a). The tangent stiffness matrix for the structure $[K_T]$ may then be found by assembling the condensed element tangent stiffness matrices. After the condensed displacement vector is determined, the complete set of nodal displacements can be recovered. This condensation and recovery procedure is necessary for the analysis to be applicable to segmented or branched shells featuring slope discontinuities.

3. The load-disturbance method

3.1. General

It is well known that for many shells, the deformation mode changes during the postbuckling process. This phenomenon is often referred to as mode switching or mode jumping (e.g. Riks et al., 1996; Stein, 1959; Supple, 1970). Mode switching is associated with re-bifurcation (secondary or higher order bifurcation points) along the path of deformation, and is a challenge to numerical analysts (e.g. Choong and Ramm, 1998; Kheyrkhahan and Peek, 1999; Kusher, 1997; Riks et al., 1996). For shells of revolution, re-bifurcation is characterized by the appearance of additional harmonic modes. These additional modes are generally different from those from nonlinear coupling, so they do not appear automatically. In order for postbuckling mode changes to be followed, it is necessary to disturb the shell into these additional modes.

A method for postbuckling analysis is thus presented here, which has the ability to follow postbuckling paths involving mode switching. In this method, a postbuckling analysis is converted into a conventional nonlinear analysis by including small loads of appropriate distributions in the analysis. This method is called the load-disturbance method. The load-disturbance concept is not new. For example, Chan and Trbojevic (1977) used the load-disturbance method to determine buckling loads using a nonlinear analysis. A difficulty with the load-disturbance method in general for postbuckling analysis is that the specification of load-disturbances of a particular form of distribution which can guide the structure into the lowest postbuckling path or a controlled deformation mode may not be straightforward. More specifically, if general shell elements are used to model a perfect shell of revolution without the imposition of additional constraints, the shell with very small pre-defined load-disturbances are subject to the influence of accumulated random or systematic errors and its postbuckling deformation mode cannot be controlled to understand more switching and interaction. For example, for a general shell element, when small loads in a number of pre-defined harmonic modes need to be applied, the summation of these harmonic loads is represented with approximation errors as equivalent nodal loads. As a result, systemic approximation errors are introduced which can introduce extra harmonic modes into the deformations of the shell. This difficulty automatically disappears when a semi-analytical coupled-harmonics formulation (Hong and Teng, 2002) for the nonlinear non-symmetric deformation of shells of revolution is applied to the postbuckling analysis of axisymmetrically loaded shells of revolution as deformations are described by a set of pre-defined harmonic modes. Disturbances can be easily included in all harmonics which are likely candidates for postbuckling deformations. This leads to a simple and effective approach for tracing complex postbuckling paths involving mode switching, a phenomenon which is very difficult to capture using general shell elements. However, no previous study appears to have combined the load-disturbance method with a semi-analytical nonlinear analysis of shells of revolution to model postbuckling mode switching as presented here. It should be noted that a semi-analytical formulation for shells of revolution based on the pseudo-load method (e.g. Wunderlich et al., 1985, 1989) cannot be applied with the load-disturbance method for postbuckling analysis, as the pseudo-load treatment prevents the analysis from following any unstable postbuckling path.

While mode switching has been quite widely documented in the existing literature, there has been little information on mode interaction. Almost all previous researchers have assumed, often implicitly, that mode switching from one to another occurs suddenly, and this assumption is behind the approach of establishing the actual postbuckling path by drawing a lower bound festoon curve to the postbuckling curves of several deformation modes (e.g. Esslinger and Geier, 1975; Schmidt et al., 1998). In fact, significant interaction between different modes exists, and this lower bound approach is invalid. This aspect is illustrated in the numerical examples described below.

3.2. Specification of load-disturbance

In the load-disturbance method, small non-symmetric loads in N selected harmonics are added to the axisymmetric loads to guide the shell into the postbuckling path. For any given external load component F (distributed forces in the normal, circumferential and meridional directions or concentrated forces in the radial, circumferential and axial directions and concentrated meridional moment), the total value of the component is

$$F = F_0 + \sum_{i}^{N} (\xi_i F_0 \cos n_i \theta) \tag{8}$$

in which F_0 is the actual value of this load component and is axisymmetric, n_i is the harmonic number of the ith mode, ξ_i is the disturbance factor for harmonic mode n_i and the value of ξ_i is usually set to be less than 10^{-4}.

To trace the postbuckling path with the shell deforming in a single chosen harmonic mode, the external loads (Eq. (8)) are given by

$$F = F_0 + \xi F_0 \cos n\theta \tag{9}$$

With these applied loads, the axisymmetric analysis problem is converted into a non-symmetric analysis problem. The nonlinear finite element formulation described in Hong and Teng (2002) can be used directly for postbuckling analysis using the load-disturbance method. Before the applied load reaches the bifurcation load, the shell follows the axisymmetric pre-buckling path. Because the value of ξ is generally set to be less than 10^{-4}, the influence on the pre-buckling deformations of the small non-symmetric loads is usually very small. When the applied load approaches the bifurcation load, the solution will continue to the postbuckling path. Many numerical examples are given later to demonstrate the validity of this approach.

3.3. Handling postbuckling mode switching and interaction

It is generally believed that mode switching of shells leads to reductions in the number of waves (e.g. Kato et al., 1997). Based on this information, a postbuckling analysis including the critical mode n_{cr} and a number of lower modes $n_{cr} - 1$, $n_{cr} - 2$, etc. is suitable for tracing the postbuckling path considering mode switching. To explain more clearly how postbuckling mode switching and interaction are modelled using the load-disturbance method, a postbuckling analysis retaining only two non-symmetric terms in Eq. (8) may be considered. The first one is the critical harmonic mode n (or any other mode if so desired) with the second being the harmonic mode $n - 1$. Then, Eq. (8) can be written as

$$F = F_0 + \xi_n F_0 \cos n\theta + \xi_{n-1} F_0 \cos(n-1)\theta \tag{10}$$

in which the values of ξ_n and ξ_{n-1} are usually set to be less than 10^{-4}. As has been shown in Hong and Teng (2002), nonlinear coupling has only a limited influence in many cases, particularly in the early stage of postbuckling deformations. The higher modes $2n$ and $3n$ for harmonic mode n from nonlinear coupling, and higher modes $2(n-1)$ and $3(n-1)$ for harmonic $n-1$ from nonlinear coupling are therefore not included in the analysis as the objective here is to investigate mode switching and interaction along the postbuckling path. However, harmonic mode 1 due to nonlinear coupling between harmonic modes n and $n-1$ needs to be retained in the analysis for some problems, in order to achieve more rapid convergence to equilibrium states. No disturbance needs to be included in harmonic mode 1 as non-zero displacements in this mode appear naturally from nonlinear coupling (Hong and Teng, 2002).

With the applied loads given by Eq. (10), the postbuckling path can continue to the secondary postbifurcation path following a mode change. The value of ξ_{n-1} is usually less than 10^{-4}, and such a small

value ensures that the shell is guided into the secondary bifurcation path or mode interaction without introducing undesirable influence on the primary bifurcation path. Several numerical examples are presented below to demonstrate the validity and capability of the present method.

4. Numerical examples

4.1. General

The load-disturbance method of postbuckling analysis presented above was coded into the CHASH program (Hong and Teng, 2002). The computer program was then applied to study the postbuckling behavior of a number of typical problems. All results presented in this paper were obtained with $\xi = 10^{-5}$ for the load-disturbances unless otherwise specified. Where higher modes (modes $2n$, $3n$, etc.) due to nonlinear coupling are considered, the values of ξ were set to be 0 for these higher modes as non-zero displacements in these modes arise naturally during the analysis. In the present study, the peak load or the load at which the buckling mode starts to grow is referred to as the buckling load for appropriate differentiation from "the bifurcation load" which is reserved for the precise bifurcation load from a non-symmetric bifurcation analysis using the NEPAS program (Teng and Rotter, 1989b). In this terminology, the buckling load is slightly below the bifurcation load due to the influence of small non-symmetric load disturbances. All three-dimensional deformed shapes are plotted using normal displacements only.

The arc-length method (Crisfield, 1981; Ramm, 1981; Riks, 1979) was included in the CHASH program (Hong and Teng, 2002) for nonlinear analysis. It should be noted that even with the arc-length method, difficulty in convergence may be encountered in the vicinity of a bifurcation point around which the load–displacement curve features a sharp turn. Reductions in the load step size are generally required in such situations. While in the present study, user intervention was used when necessary, an automated procedure is probably more desirable. This aspect is however beyond the scope of the present study and not further discussed.

4.2. Spherical cap under uniform pressure

The postbuckling analysis of a clamped spherical cap under uniform external pressure which was studied by Kato et al. (1997) is considered here. The cap has a rise parameter $\lambda = 7$, which is defined by

$$\lambda = 2\sqrt[4]{3(1-\nu^2)}\cdot\sqrt{H/t} \tag{11}$$

The results presented in Fig. 2 are all for a Poisson's ratio $\nu = 0.3$, with the vertical axis being the load normalized by the classical buckling pressure of a corresponding spherical shell under uniform pressure which is defined by

$$q_{\mathrm{cr}} = \frac{2Et^2}{R^2\sqrt{3(1-\nu^2)}} \tag{12}$$

Fig. 2a shows the postbuckling path of the cap predicted by the present method for harmonic mode 3 with two higher harmonic modes (6 and 9) due to nonlinear coupling taken into account. This predicted path is seen to be in close agreement with that of Kato et al. (1997), showing that the present method produces accurate results.

Fig. 2b compares the multi-mode postbuckling path for $n = 1 + 2 + 3$ with the postbuckling paths for individual harmonic modes, in which the horizontal axis is the vertical displacement normalized by the shell thickness at a point with its circumferential angular coordinate $\theta = 0$ and the radial coordinate $r = 0.5r_0$, where r_0 is the base radius of the cap. The multi-mode curve does not follow the lower bound of the

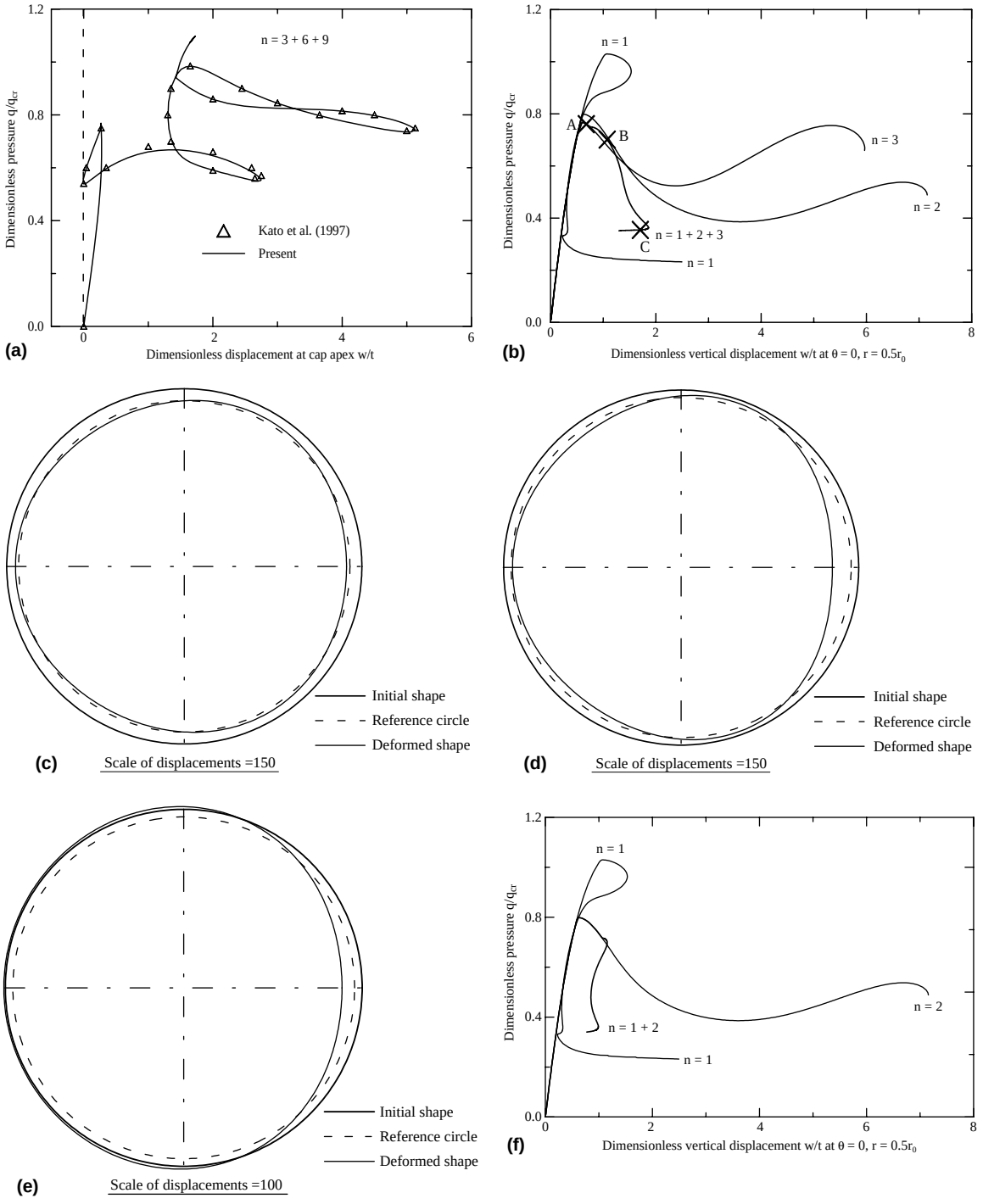

Fig. 2. Spherical cap under uniform external pressure. (a) Postbuckling path of $n = 3 + 6 + 9$. (b) Effect of mode switching and interaction. (c) Deformed circumference at $r = 0.5r_0$ at point A in (b). (d) Deformed circumference at $r = 0.5r_0$ at point B in (b). (e) Deformed circumference at $r = 0.5r_0$ at point C in (b). (f) Effect of mode switching and interaction.

postbuckling curves for the individual harmonic modes, showing that strong interaction exists between the three harmonic modes. Only in the early postbuckling stage does the multi-mode curve follow the path for harmonic mode 3 and then that for harmonic mode 2 briefly. Even here, it is surprising to see that the multi-mode path switches to the higher path for harmonic mode 2 instead of continuing along the lower path for harmonic mode 3 until it intersects the path for harmonic mode 2. The path for harmonic mode 1 is much lower than those for both harmonic modes 2 and 3 in most of the deformation range considered here, but the multi-mode path does not reach the path for harmonic mode 1 even though harmonic mode 1 becomes important in the late stage of postbuckling deformations. Deformed circumferences for three points (A, B and C) along the multi-mode path are plotted in Fig. 2c–e. In these figures, a suitably positioned reference circle (dashed line) is plotted to show the circumferential waves more clearly. Three circumferential waves are found in the deformations at point A (Fig. 2c). With further deformations, re-bifurcation occurs and the predominant harmonic mode gradually changes. The deformations of the spherical cap at the secondary postbuckling state B (Fig. 2d) show this change, where the number of the predominant circumferential waves is two. At point C, one circumferential wave is clearly seen (Fig. 2e). The changes in the number of circumferential waves from 3, to 2 and then 1 are gradual.

The postbuckling path for $n = 1 + 2$ is shown in Fig. 2f. Because harmonic mode 3 is excluded, the two-mode pre-buckling path initially follows the postbuckling path for harmonic mode 2. With further deformations, deformed shapes of the shell not shown here indicated that re-bifurcation occurs and the predominant harmonic mode gradually changes from 2, to 1 and then 0 (axisymmetric).

4.3. Cylindrical shell under axial compression

The present method was also applied to a circular cylindrical shell under axial compression which is one of the many cylindrical shells studied by Yamaki (1984). The shell has geometric properties of $R = 405$ mm, thickness $t = 1$ mm, and length $L = 291.18$ mm and material properties of elastic modulus $E = 5.56$ GPa, and Poisson's ratio $v = 0.3$. The Batdorf parameter of the cylinder $Z\ (= L^2\sqrt{1 - v^2}/Rt)$ is 200. In the present study, both ends of the cylinder were clamped with the top end allowed to move axially so that axial compression could be applied. This differs slightly from that assumed by Yamaki (1984) in his analytical study in which both ends were restrained against all displacements.

The postbuckling paths for individual harmonic modes are shown in Fig. 3a in which the vertical axis represents the applied axial stress normalized by the classical buckling stress given by

$$\sigma_{\mathrm{cl}} = \frac{Et}{R\sqrt{3(1 - v^2)}} \tag{13}$$

while the horizontal axis is the end shortening of the shell. The disturbance factors are $\xi_i = 10^{-6}$ ($i =$ 14–18). The buckling loads and characteristic postbuckling loads for various harmonic modes are listed in Table 1.

The multi-mode postbuckling path for $n = 1 + 15 + 16$ is plotted in Fig. 3b. Here the disturbance factors are: $\xi_{15} = \xi_{16} = 10^{-4}$. The characteristic postbuckling load of this path is 0.3756_{cl}, which is between the postbuckling loads of modes 15 and 16 (Table 1). Fig. 3c and d show the deformed circumferences at a height of $0.6\,L$ ($L =$ total height of the cylinder) at two postbuckling states (Points A and B in Fig. 3b). The number of circumferential waves is seen to change from 16 to 15. Since the buckling loads of harmonic modes 15 and 16 are close to each other, this mode change is not very clear and involves interaction between the two modes.

The postbuckling path for $n = 16 + 17$ is plotted in Fig. 3e, which was obtained with $\xi_{16} = \xi_{17} = 10^{-4}$. This curve is the same as the postbuckling path of harmonic mode 16. The deformed circumferences at a height of $0.6\,L$ of the shell at two postbuckling states (Points A and B in Fig. 3e) are shown in Fig. 3f and g. No mode change is seen during the postbuckling process. That is, harmonic mode 17 has no influence on

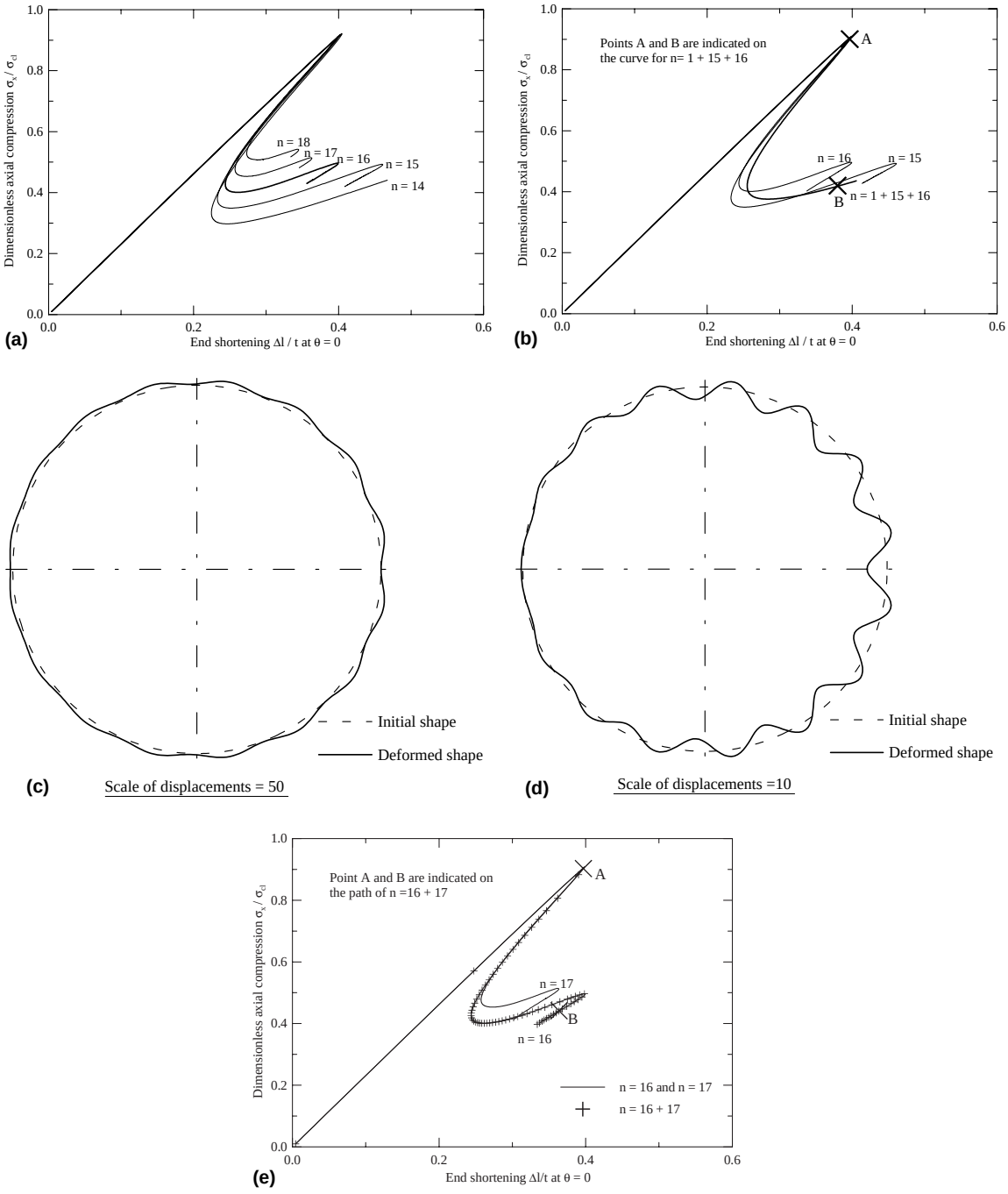

Fig. 3. Cylindrical shell under axial compression. (a) Postbuckling paths of various harmonic modes. (b) Effect of mode switching and interaction. (c) Deformed circumference at $0.6L$ at point A in (b). (d) Deformed circumference at $0.6L$ at point B in (b). (e) Postbuckling paths of $n = 16$, $n = 17$, $n = 16 + 17$. (f) Deformed circumference at $0.6L$ at point A in (e). (g) Deformed circumference at $0.6L$ at point B in (e).

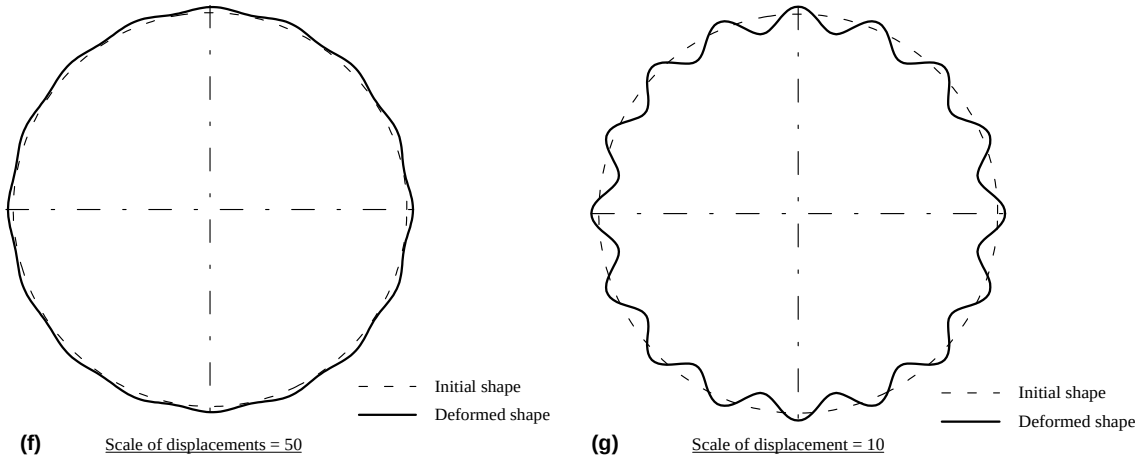

Fig. 3 (*continued*)

Table 1
Buckling loads and characteristic postbuckling loads of a cylindrical shell under axial compression

Harmonic mode n	Bifurcation analysis $n_{cr} = 16$	14	15	16	17	18
Buckling load (σ_b/σ_{cl})	0.9110	0.9222	0.9124	0.9089	0.9176	0.9176
Postbuckling load (σ_p/σ_{cl})	–	0.3000	0.3493	0.4010	0.4540	0.5070

the postbuckling path of harmonic mode 16. This supports the observation that re-bifurcation is associated with reductions in the number of circumferential waves in the postbuckling process of shells.

In Fig. 3a, b and e, a reversal in the elongation of the postbuckling curve is seen for some of the postbuckling paths. The deformations of the shell near these reversals were examined and it was found these reversals were due to a deformation mode change in the meridional direction.

4.4. Cylindrical shell under uniform external pressure

A cylindrical shell under uniform external pressure previously analyzed by Bulenda (1993) was next investigated. The cylinder is restrained against both radial and meridional displacements at the two ends. It is further restrained against axial displacements at the mid-height so that rigid body translations in the axial direction are excluded. The material and geometric properties of the shell are: elastic modulus $E = 3 \times 10^4$ KN/m^2, Poisson's ratio $v = 0$, radius $R = 100$ m, height $H = 140$ m, and thickness $t = 2$ m.

Fig. 4a shows the present results in comparison with those from Bulenda (1993) and Eckstein (1983) for the postbuckling path considering the critical mode and the next higher mode from nonlinear coupling. It can be seen that the present method produces identical results which are much closer to those of Eckstein (1983) than those of Bulenda (1993). $\xi = 10^{-6}$ was used in this problem. The postbuckling paths for various harmonic modes found using the present method ($\xi_5 = \xi_6 = \xi_7 = 10^{-6}$) are plotted in Fig. 4b. For this shell, the buckling loads for buckling modes 5 and 7 are significantly different from the critical buckling load p_{cr} for $n_{cr} = 6$.

The multi-mode postbuckling path for $n = 1 + 5 + 6$ is compared to postbuckling paths for harmonic modes 5, 6 and 7 in Fig. 4c. The smooth transition seen near the limit point in these curves is due to the use of slightly larger disturbance factors ($\xi_5 = \xi_6 = \xi_7 = 10^{-3}$). When a value equal to or less than 10^{-4}

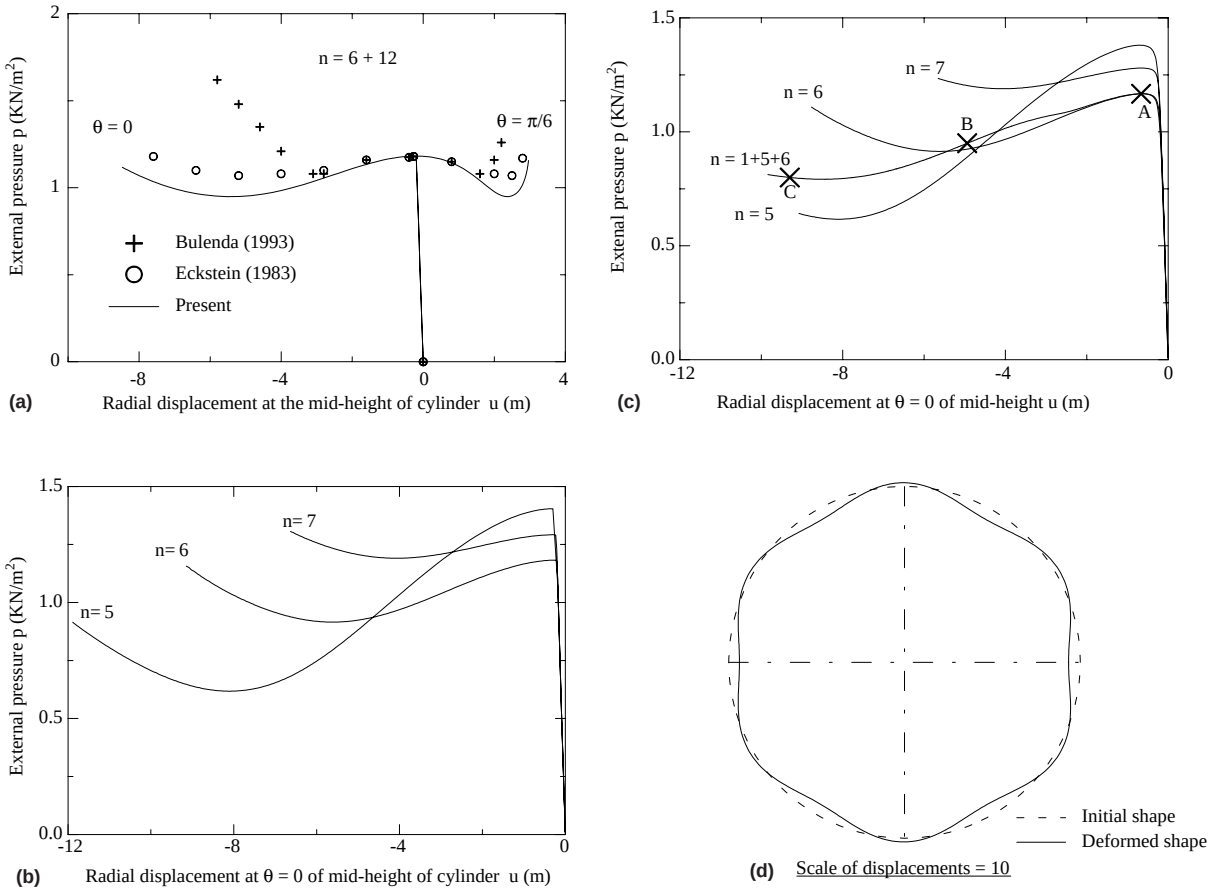

Fig. 4. Cylindrical shell under uniform external pressure. (a) Postbuckling paths of $n = 6 + 12$. (b) Postbuckling paths of various harmonic modes. (c) Effect of mode switching and interaction. (d) Deformed circumference at mid-height at point A in (c). (e) Deformed circumference at mid-height at point B in (c). (f) Deformed circumference at mid-height at point C in (c). (g) Deformed shape at point A in (c). (h) Deformed shape at point C in (c).

was set for the disturbance factors ξ_5 and ξ_6, the multi-mode postbuckling path could be followed well only in the early postbuckling stage. In the advanced postbuckling stage, it was very difficult to achieve convergence. The larger disturbance factors have little effect on the predicted postbuckling path except for a small effect near the bifurcation point with the peak load for harmonic mode 6 being 98.7% of the bifurcation load (Table 2). The characteristic postbuckling loads for various harmonic modes are also given in Table 2. It shows that the characteristic postbuckling load obtained for $n = 1 + 5 + 6$ is between those of harmonic modes 5 and 6. The difference between these loads is significant. Due to mode interaction, the postbuckling path for $n = 1 + 5 + 6$ follows that of harmonic mode 6 only in the initial stage of postbuckling deformation, but then deviates from it; the multi-mode curve does not follow the postbuckling path for harmonic mode 5 at all, despite that the latter lies below the former.

The deformed circumference at the mid-height of the postbuckled cylindrical shell is plotted for three deformation states (Points A, B and C in Fig. 4c) in Fig. 4d–f. These plots show clearly the changes in the number of circumferential waves due to mode switching. Three-dimensional plots of the shell at two postbuckling states (Points A and C in Fig. 4c) are given in Fig. 4g and h.

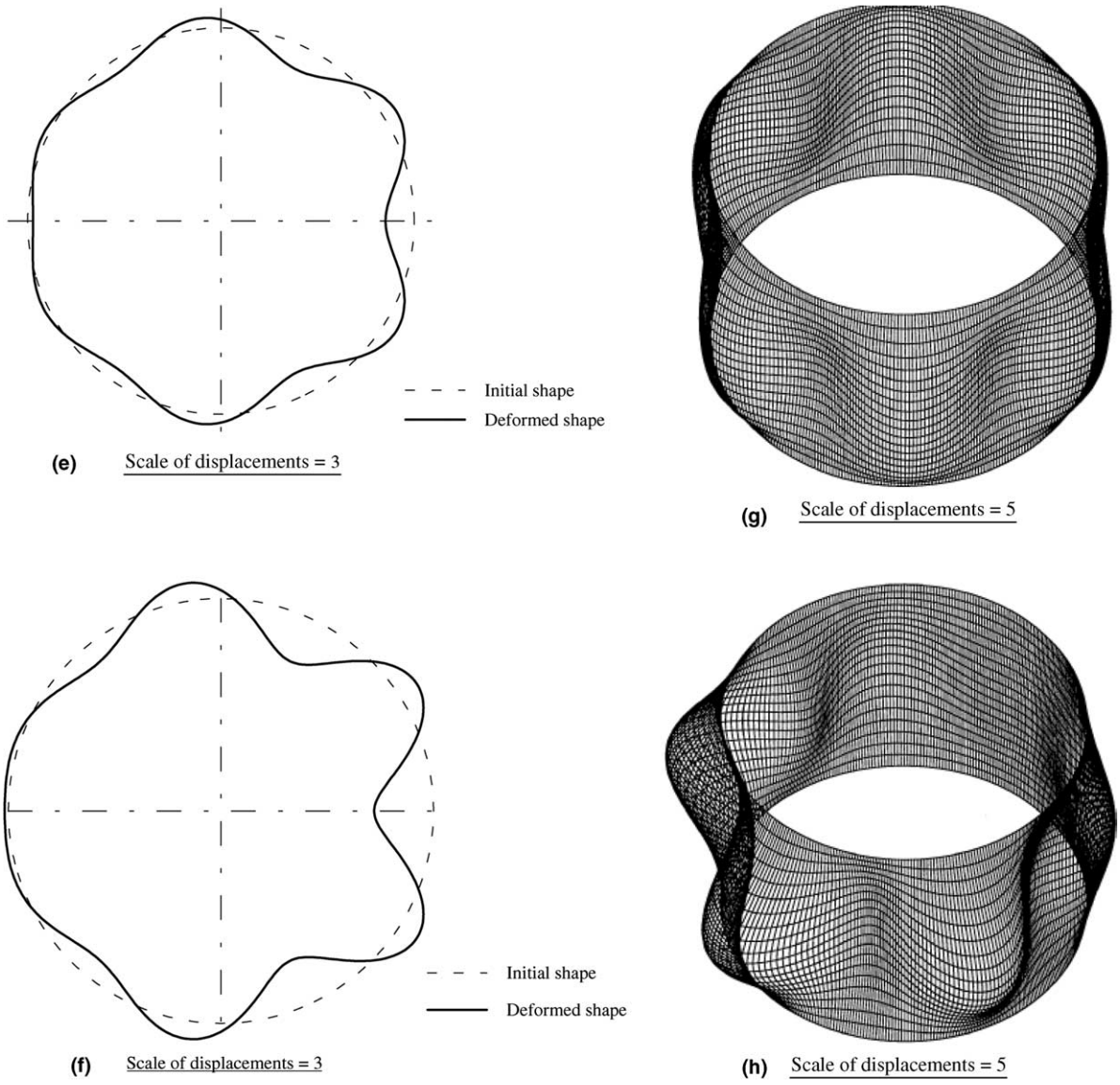

Fig. 4 (*continued*)

Table 2
Buckling loads and characteristic postbuckling loads of a cylindrical shell under external pressure

Harmonic mode n	Bifurcation analysis $n_{cr} = 6$	5	5	6	6	7	$1 + 5 + 6$
ξ_i	–	10^{-6}	10^{-3}	10^{-6}	10^{-3}	10^{-6}	10^{-3}
Buckling load p_b (KN/m^2)	1.1829	1.4038	1.3805	1.1822	1.1674	1.2918	1.1674
Postbuckling load p_p (KN/m^2)	–	0.6175	0.6169	0.9153	0.9145	1.1905	0.7919

4.5. Cylindrical shell under a radial ring load at mid-height

A cylindrical shell subject to a radial ring load is considered here. The shell has geometrical properties of length $L = 1500$ mm, radius $R = 500$ mm, and thickness $t = 1$ mm, and material properties of elastic modulus $E = 200$ GPa and Poisson's ratio $v = 0.3$. Both two ends are simply supported, with only meridional rotations permitted. A reference load $q_r = 7.56$ N/mm was used.

First, the postbuckling paths for harmonic modes 13, 14, 15, 16 and 17 were found (Fig. 5a). It can be seen that the buckling loads for these modes are close to each other (Table 3). Those for buckling modes 14 and 15 are almost identical. By contrast, the characteristic postbuckling loads for the different modes are not so close to each other.

The postbuckling curve for harmonic modes $1 + 13 + 14$ is plotted in Fig. 5b. Larger disturbance factors were found to be necessary in order to trace the advanced portion of this mutli-mode postbuckling path, so $\xi_{13} = \xi_{14} = 10^{-3}$ were used. As a result, the peak of the multi-mode curve shows a smooth transition with a

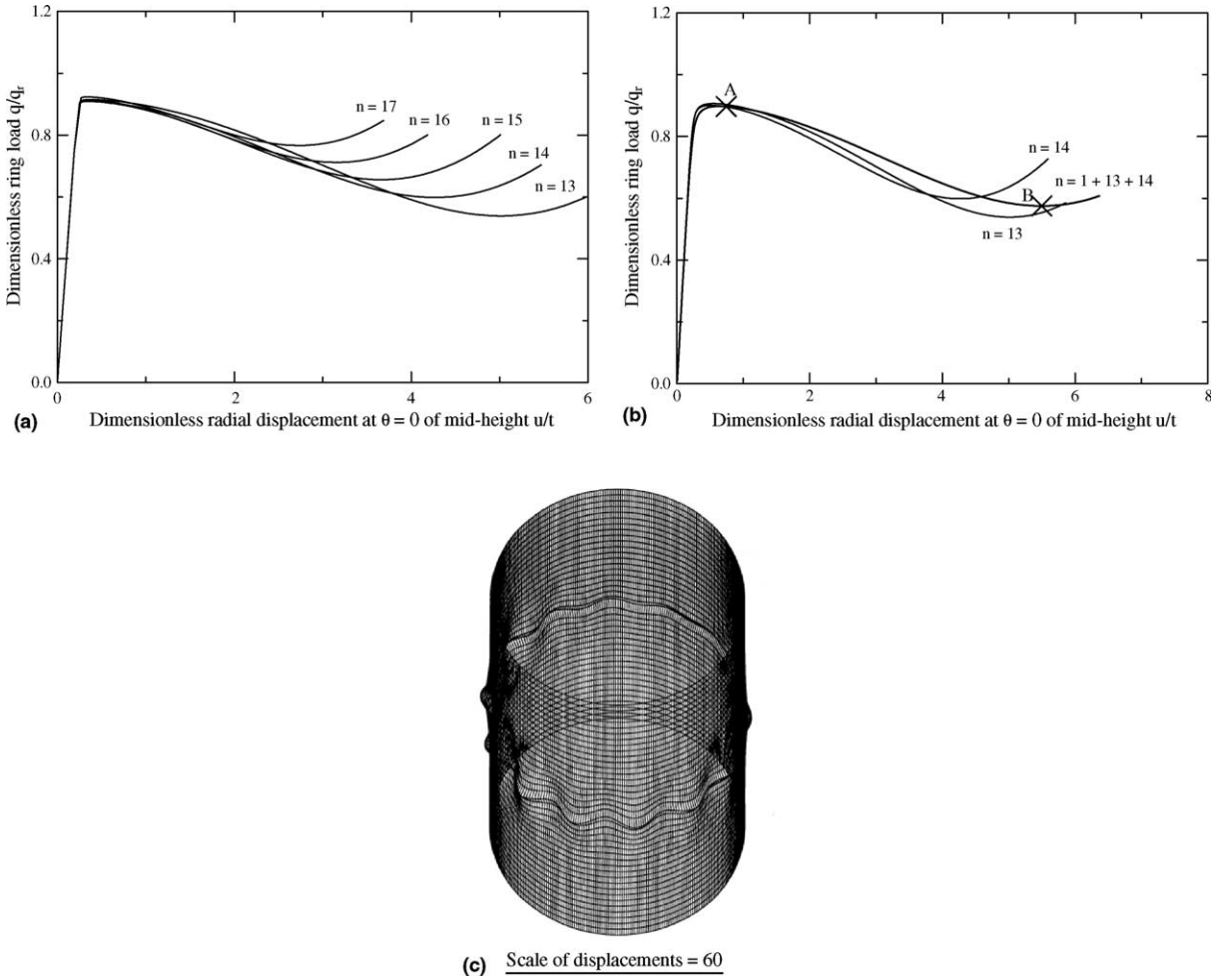

Fig. 5. Cylindrical shell under a radial ring load. (a) Postbuckling paths of various harmonic modes. (b) Effect of mode switching and interaction. (c) Deformed shape at point A in (b).

Table 3
Buckling loads and characteristic postbuckling loads of a cylindrical shell under a radial ring load at mid-height

Harmonic mode n	13	14	15	16	17	13	14	1 + 13 + 14
ξ_i	10^{-5}	10^{-5}	10^{-5}	10^{-5}	10^{-5}	10^{-3}	10^{-3}	10^{-3}
Buckling load q_b/q_r	0.9155	0.9099	0.9094	0.9140	0.9239	0.9060	0.9007	0.8976
Postbuckling load q_p/q_r	0.5392	0.5988	0.6562	0.7122	0.7669	0.5372	0.5988	0.5752

Note: critical bifurcation mode $n_{cr} = 15$, bifurcation load $q_b/q_r = 0.9118$.

peak load being 1.56% smaller than the bifurcation load for the critical mode. (Table 3). The multi-mode path does not follow either the path for mode 13 nor the path for mode 14, and is above the paths for both modes 13 and 14 over a large range. The characteristic postbuckling load of this multi-mode path is less than that for $n = 14$, but larger than that for $n = 13$ (Table 3). A three-dimensional view at the postbuckling state A is shown in Fig. 5c.

5. Conclusions

Based on the coupled-harmonics finite element formulation for the nonlinear analysis of elastic shells of revolution subject to non-symmetric loads (Hong and Teng, 2002), a numerical method for the advanced postbuckling analysis of perfect thin shells of revolution subject to axisymmetric loads has been presented. In this method, by specifying small load-disturbances in appropriate harmonic modes, complex postbuckling paths with mode switching and interaction can be predicted.

The present method was applied to several typical numerical examples to demonstrate its capability. Numerical results show that the small load disturbances have practically no influence on the predicted response in most cases as these disturbances can be made very small. In a small number of cases when mode interaction is considered, the load disturbances may need to be slightly larger, which can then have a small influence on the accuracy of the predicted buckling load and the postbuckling path in its vicinity.

In general, the present results are in close agreement with the limited existing results. The existing belief that re-bifurcation of shell structures leads to reductions in the number of circumferential waves is confirmed by the present numerical results. A significant conclusion from the present numerical study is that mode switching does not occur suddenly. Instead, there is strong interaction between different modes and the transition of deformation mode from one to another is gradual. Consequently, the conventional approach (e.g. Esslinger and Geier, 1975; Schmidt et al., 1998) of finding the postbuckling path of a shell as the lower festoon curve of postbuckling paths of individual harmonic modes is not valid and is at best a convenient approximation.

Acknowledgements

Both authors are grateful to The Hong Kong Polytechnic University and the Research Grants Council of the Hong Kong Special Administrative Region (Project No. PolyU 5045/98E) for their financial support.

References

Azrar, L., Cochelin, B., Damil, N., Potier-Ferry, M., 1993. An asymptotic-numerical method to compute the postbuckling behaviour of elastic plates and shells. International Journal for Numerical Methods in Engineering 36, 1251–1277.

Budiansky, B., Hutchinson, J.W., 1966. A survey of some buckling problems. AIAA Journal 4, 1505–1510.
Bulenda, T., 1993. Harmoni-by-harmonic method for the postcritical computation of axisymmetric shells. In: Valliappan, Pulmano, Tin-Loi (Eds.), Computational Mechanics. Balkema, Rotterdam, pp. 43–48.
Chan, A.S.L., Trbojevic, V.M., 1977. Thin shell finite element by the mixed method formulation—Parts 2 and 3. Computer Methods in Applied Mechanics and Engineering 10, 75–103.
Choong, K.K., Ramm, E., 1998. Simulation of buckling process of shells by using the finite element method. Thin-Walled Structures 31, 39–72.
Combescure, A., 1999. Are the static postbuckling predictions conservative? In: Proceedings of the Second International Conference on Advanced in Steel Structures, Hong Kong, pp. 713–720.
Crisfield, M.A., 1981. A fast increment/iterative solution procedure that handles snap-through. Computer and Structures 13, 55–62.
Eckstein, U., 1983. Nichtlineare Stabilitatsberechnung elastischer Schalentragwerke. Technical Report No. 83-3, Ruhr-Universitat Bochum, Mitteilung.
Endou, A., Hangai, Y., Kawamata, S., 1976. Post-buckling analysis of elastic shells of revolution by the finite element method. Report of the Institute of Industrial Science, The University of Tokyo.
Esslinger, M., Geier, B., 1975. Postbuckling Behavior of Structures. Springer-Verlag.
Flores, F.G., Godoy, L.A., 1992. Elastic postbuckling analysis via finite element and perturbation techniques Part I: Formulation. International Journal for Numerical Methods in Engineering 33, 1775–1794.
Flores, F.G., Godoy, L.A., 1993. Elastic postbuckling analysis via finite element and perturbation techniques Part II: Application to shells of revolution. International Journal for Numerical Methods in Engineering 36, 331–354.
Guggenberger, W., 1996. Analysis of the torsional postbuckling mode of externally pressurized circular cylindrical shells. In: European Workshop on Thin-Walled Steel Structures, September 25–28, Krzyzowa, Poland.
Hong, T., Teng, J.G., 2002. Nonlinear analysis of shells of revolution under arbitrary loads. Computer and Structures 80, 1547–1568.
Kato, S., Chiba, Y., Mutoh, I., 1997. Secondary buckling analysis of spherical caps. Structural Engineering and Mechanics 5, 715–728.
Kheyrkhahan, M., Peek, R., 1999. Postbuckling analysis and imperfection sensitivity of general shells by the finite element method. International Journal of Solids and Structures 36, 2641–2681.
Koiter, W.T., 1945. Over de Stabiliteit van het Elastisck Evenwich (On the stability of elastic equilibrium). Ph.D. Thesis, Delft University, English translation issued as NASA TT F-10, 1967.
Kusher, A., 1997. Bifurcation buckling eigenvector characteristics for structures exhibiting buckling mode interaction. Computer Methods in Applied Mechanics and Engineering 149, 89–100.
Ramm, E., 1981. Strategies for tracing nonlinear response near limit points. In: Wunderlich, W., Stein, E., Bathe, K.J. (Eds.), Nonlinear Finite Element Analysis in Structural Mechanics. Springer-Verlag, New York, pp. 63–89.
Riks, E., 1979. An incremental approach solution of snapping and buckling problems. International Journal of Solids and Structures 15, 524–551.
Riks, E., Rankin, C.C., Brogan, F.A., 1996. On the solution of mode jumping phenomena in thin-walled shell structures. Computer Methods in Applied Mechanics and Engineering 136, 59–92.
Rotter, J.M., Jumikis, P.T., 1988. Nonlinear strain–displacement relations for thin shells of revolution. Research Report R563, School of Civil and Mining Engineering, University of Sydney, Australia.
Schmidt, H., Binder, B., Lange, H., 1998. Postbuckling strength design of open thin-walled cylindrical tanks under wind load. Thin-Walled Structures 31, 203–220.
Shen, H.S., 1996. Postbuckling analysis of cylindrical shells under combined external liquid pressure and axial compression. Thin-Walled Structures 25, 297–317.
Shen, H.S., Chen, T.Y., 1991. Buckling and postbuckling behavior of cylindrical-shells under combined external-pressure and axial compression. Thin-Walled Structures 12, 321–334.
Stein, M., 1959. The phenomenon of change of buckling patterns in elastic structures. NASA Technical Report R-39.
Supple, W.J., 1970. Changes of wave-form of plates in the post-buckling range. International Journal of Solids and Structures 6, 1243–1258.
Teng, J.G., Hong, T., 1998. Nonlinear thin shell theories for numerical buckling predictions. Thin-Walled Structures 31, 89–115.
Teng, J.G., Rotter, J.M., 1989a. Elastic–plastic large deflection analysis of axisymmetric shells. Computers and Structures 31, 211–233.
Teng, J.G., Rotter, J.M., 1989b. Non-symmetric bifurcation of geometrically nonlinear elastic–plastic axisymmetric shells under combined loads including torsion. Computers and Structures 32, 453–475.
Wunderlich, W., Cramer, H., Obrecht, H., 1985. Application of ring elements in the nonlinear analysis of shells of revolution under nonaxisymmetric loading. Computer Methods in Applied Mechanics and Engineering 51, 259–275.

Wunderlich, W., Obrecht, H., Springer, H., Lu, Z., 1989. A semi-analytical approach to the nonlinear analysis of shells of revolution. In: Noor, A.K., Belytschko, T., Simo, J.C. (Eds.), Analytical and Computational Models for Shell. ASME, New York, pp. 505–536.

Yamaki, N., 1984. Elastic Stability of Circular Cylindrical Shells. North-Holland.